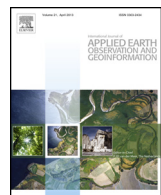




Contents lists available at ScienceDirect

International Journal of Applied Earth Observation and Geoinformation

journal homepage: www.elsevier.com/locate/jag



Retrieving canopy height and density of paddy rice from Radarsat-2 images with a canopy scattering model



Yuan Zhang^{a,*}, Xiaohui Liu^b, Shiliang Su^c, Cuizhen Wang^d

^a Key Laboratory of Geographical Information Science, Ministry of Education, East China Normal University, Shanghai 200241, China

^b Key Laboratory of Wetland Ecology and Environment, Northeast Institute of Geography and Agroecology, CAS, Changchun 130102, China

^c School of Resource and Environmental Sciences, Wuhan University, Wuhan 430079, China

^d Department of Geography, University of South Carolina, Columbia, SC 29208, USA

ARTICLE INFO

Article history:

Received 12 September 2013

Accepted 3 December 2013

Keywords:

Radarsat-2

Canopy scattering model

Paddy rice

Canopy height and density

ABSTRACT

Quantification of rice biophysical properties is important not only for rice growth monitoring and cropping management, but for understanding carbon cycle in agricultural ecosystems. In this study, a rice canopy scattering model (RCSM) was firstly utilized to simulate rice backscatter with a root mean square error (RMSE) <1 dB in comparison with the C-band, HH-polarization Radarsat-2 images. And then, by integrating the model with a generic algorithm optimization tools (GOAT), canopy height and density were separately retrieved from Radarsat-2 images acquired in three rice growth stages (elongation stage, heading stage and yellow ripening stage). Accuracy analysis showed that the two parameters could be retrieved with the RMSE of 5.4 cm in height, and 26 (#/m²) in density. The study demonstrated the potential of Radarsat-2 SAR data for quantitative mapping of biophysical parameters of paddy rice.

© 2013 Elsevier B.V. All rights reserved.

1. Introduction

Rice cropping is one of the major agricultural activities in China. Rapid population growth demands higher rice production. In South and Southeast China, agricultural land use has been dramatically replaced by urban build-ups accompanying fast economic development in the past decades (Lin and Ho, 2003; Wu et al., 2009; Su et al., 2011). Croplands for rice cultivation in Northeast China, however, have been increasing since the 1990s (National Bureau Statistics of China, 1990, 2000, 2013; Zhang et al., 2012). Single-season paddy rice is the staple food crop and is widely planted in Northeast China (Frolking et al., 2002). Accounting for 14% of the country's total rice cropping areas, this region has become one of major food providers in China (National Bureau Statistics of China, 2013). Therefore, real-time, reliable rice monitoring in this region has particular significance for steady food provision for the country.

Monitoring rice production with remote sensing technique has been widely carried out in many countries of Southeast Asia (Fang, 1998; Okamoto and Kawashima, 1999; Xiao et al., 2005; Nuarsa et al., 2012). However, frequent cloud cover and rainfall during rice growth season are often challenging to optical remote sensing. Synthetic aperture radar (SAR), due to its all-weather, day-and-night observation capabilities, becomes an important alternative

in rice studies (Panigrahy et al., 1999; Oza et al., 2008; Zhang et al., 2011). Many SAR systems have been launched in the past two decades, including ERS-1/2 (launched in 1991/1995), JERS-1 (1992), RADARSAT-1/2 (1995 and 2007), ENVISAT (2002), ALOS-PALSAR (2006), TerraSAR and COSMO-SkyMed (2007). Acquired from these sensors, multi-temporal, multi-polarization SAR images have been widely employed to map rice planting area and to monitor rice growth (Le Toan et al., 1997; Ribbes and Le Toan, 1999; Shao et al., 2001; Li et al., 2003; Chakraborty et al., 2005; Zhang et al., 2009; Bouvet and Le Toan, 2011; Yonezawa et al., 2012; Koppe et al., 2013).

Radar backscatter depends on geometric and physical features of scatterers interacting with SAR signal (Inoue et al., 2002). Previous studies indicate that rice biophysical attributes, e.g. leaf area index (LAI), fresh biomass, and plant height, are closely correlated with backscattering coefficients (Shao et al., 2002; Chen et al., 2006; Wang et al., 2009). Canopy height and density are the two fundamental biophysical attributes of rice development and control factors to estimate biomass. Spatio-temporal variations in rice canopy height and density at different growth stages are closely related to total leaf area of rice paddy that can be reflected by corresponding SAR images. Therefore, modeling the radiative transfer of SAR beam within rice canopy is important to better understanding the rice canopy scattering mechanism.

A limited number of canopy scattering models have been developed to simulate radar backscatter characteristics of paddy rice (Tsang et al., 1995; Wang et al., 2005, 2009). The temporal variation

* Corresponding author. Tel.: +86 2154341231; fax: +86 2154341231.

E-mail address: yuan.zhang75@gmail.com (Y. Zhang).

of the radar backscatter for rice was simulated by a first-order solution of the radiative transfer equation. The modeling results were in good agreement with that observed from X-band SAR images of HH and VV polarizations (Le Toan et al., 1989). Also, a coherent scattering model with analytic wave theory was developed for calculating the backscatter from the rice canopy, the simulation results effectively interpreted the C-band Radarsat HH data for incident angles at 23° and 43° (Wang et al., 2005).

However in these above-mentioned models, rice ear was not considered/described in the scattering components of rice canopy, so they were rarely investigated at the heading stages. A rice canopy scattering model (RCSM) were developed based on first-order radiative transfer equation by simulating rice ears and stems as thin dielectric cylinders, and leaf as elliptical disks over a dielectric half-space (Wang et al., 2009). Although the model have a potential to simulate temporal L-band radar signals at various polarization mode (HH, HV and VV) for rice backscatter, the modeled backscatter coefficients (HH and HV) in sample fields did not match so well with that observed from two ALOS/PALSAR data (error of ~3 dB). Therefore, there is a pressing need to modify this microwave scattering model for accurately simulating the scattering characteristics of rice canopy at various rice growth stages.

By taking into account the structural variation of rice plants and rice fields and the coherence or phase interference between vegetative elements, identical possibility distribution function (PDF) was used for describing the leaf orientation at different growth stages was questionable. Furthermore, ground surface should not be constantly treated as a smooth water surface during the whole growth season. There was a large difference in dielectric constants of rice fields between flooding period and after drainage. From the near maturity to harvest, moisture content of rice fields decreased gradually without taking into occasional rainfall events account. This kind of variability would inevitably influence the total canopy scattering. This could explain the large simulation error at rice heading stage that reported in Wang et al. (2009). As a continuing step of Wang et al.'s work, the PDFs of rice leaves of RCSM corresponding to different growth stages would be separately constructed. When rice canopy parameters (height and density) were retrieved, changes in structure parameters and dielectric properties of rice fields would also be adjusted and be assigned in RCSM (see detail in Section 2.3.1). Nowadays, C-band SAR image is the most prevalent and commonly used microwave radar remote sensing data. This study aims to extend the application of RCSM for simulating the interaction of multi-frequency radar signals with rice canopy, and further demonstrate the potential practicability of SAR remote sensing in rice monitoring.

In this present study, three Radarsat-2 SAR images covering a representative production area in Northeast China were acquired in three rice growth stages. The study object is to (1) test the performance of RCSM simulation for C-band backscatter returns and then, (2) quantitatively estimate and map canopy height and density of paddy rice via model inversion.

2. Datasets and methods

2.1. Study area

The study area is located in Dengta City of Liaoning Province, one of the three provinces in the Northeast China (Fig. 1). As a portion of the Liaohe River Plain, it is one of the major rice cropping areas in China. Centered at 123.32° E, 41.42° N, the study area covers a total area of 1.35×10^5 hectare (ha) with a typical temperate monsoon climate. It lies at <50 m geographic elevation above sea level with a gentle and flat topographic relief. Single-season paddy rice is dominant in this area with its growing season

from late May to early October. In one growth cycle, five major development stages of rice can be observed: (1) transplanting (late May): seedlings in seedbeds are transplanted into fields; (2) tillering (June): seedlings split up and begin to develop a root system; (3) ear differentiation (early August): ear starts to reproduce; (4) heading (mid August to late September): heads begin to form; and (5) maturing (early October): ears ripen and are ready to harvest. Two major rivers, Hunhe River and Taizihe River, flow through the Plain and feed croplands with abundant water for food production. Unlike the fragmented agricultural lands in southeast China (Wang et al., 2009), total of 2.75×10^4 ha farmlands in Dengta with regular shapes are cultivated as rice plantation. The flat topography and extensive fields make this area favorable for experimental studies of SAR remote sensing in rice monitoring.

2.2. Datasets

2.2.1. Remotely sensed imagery

As shown in Fig. 1, fine beam mode, dual-polarization (HH&HV) Radarsat-2 SAR images were acquired on Jul. 28, Aug. 21, and Sep. 14, 2011. These three dates represent three rice growth stages: elongation, heading and yellow ripening, respectively. The spatial resolution of the images is 10 m with an incidence angle of 34° at the center of the 50 km swath. The SAR imagery processing software, Next ESA SAR Toolbox (NEST) 4B-1.1 (<http://nest.array.ca/web/nest>) was utilized for reading, pre-processing, and analyzing Radarsat-2 SAR data. A 3 × 3 Gamma-MAP filter (Lopes et al., 1990) was utilized to suppress speckle noises inherent in the SAR images. After radiometric calibration and reprojection, backscattering coefficient (σ^0) of each pixel was finally extracted. The output images were resampled to 30 m resolution with the nearest neighbor algorithm using a window size of 3 × 3 to reduce noises in the preprocessing steps above. Three backscattering coefficient maps were separately taken as inputs for retrieving rice parameters at each growth stages.

Two clear scenes of Landsat-7 ETM+ images (Fig. 2A and B) were acquired on Jun. 20 and Sep. 24, 2011 (i.e. transplanting and maturation stage), which were downloaded from the EarthExplorer (<http://edcns17.cr.usgs.gov/EarthExplorer/>). Although the ETM+ system has been suffering the malfunction of its scan line corrector (SLC) loss since May 2003, the SLC-off data gaps have less impact on the scene center where the study area is located. The Principal Components Transform (PCT) technique was used to fuse the 30-m multi-spectral bands and the 15-m panchromatic band of these ETM+ images (Welch and Ehlers, 1987). The two ETM+ images were then geographically registered to the Radarsat-2 SAR images with error of <15 m. As shown in Fig. 2, paddy fields in these three dates can be easily identified. Via visual interpretation, the pan-sharpened image was digitized in ArcGIS 9.3 to extract paddy rice fields in the study area.

Most paddy fields were large and in regular shapes, and were extensively distributed over the study area. A few small, fragmented parcels were only observed in the Southwest and the Southeast. The spatial distribution of paddies within this study area in 2011 was digitized by visual interpretation from the two clear ETM+ images (Fig. 2C). Taking the study object into account, the on-screen digitization process was rigorously controlled at the boundary area of rice fields. Mixed pixels on the field boundary were excluded, and only those fields containing "pure" rice pixels were abstracted. Thus the derived rice field map have the highest user's accuracy (100%) although a slight low producer's accuracy. It was observed that total 85 measurement fields in three field campaigns were correctly and precisely delineated. These digitized data then served as a mask map to exclude non-rice lands from Radarsat-2 SAR composition (Fig. 2D).

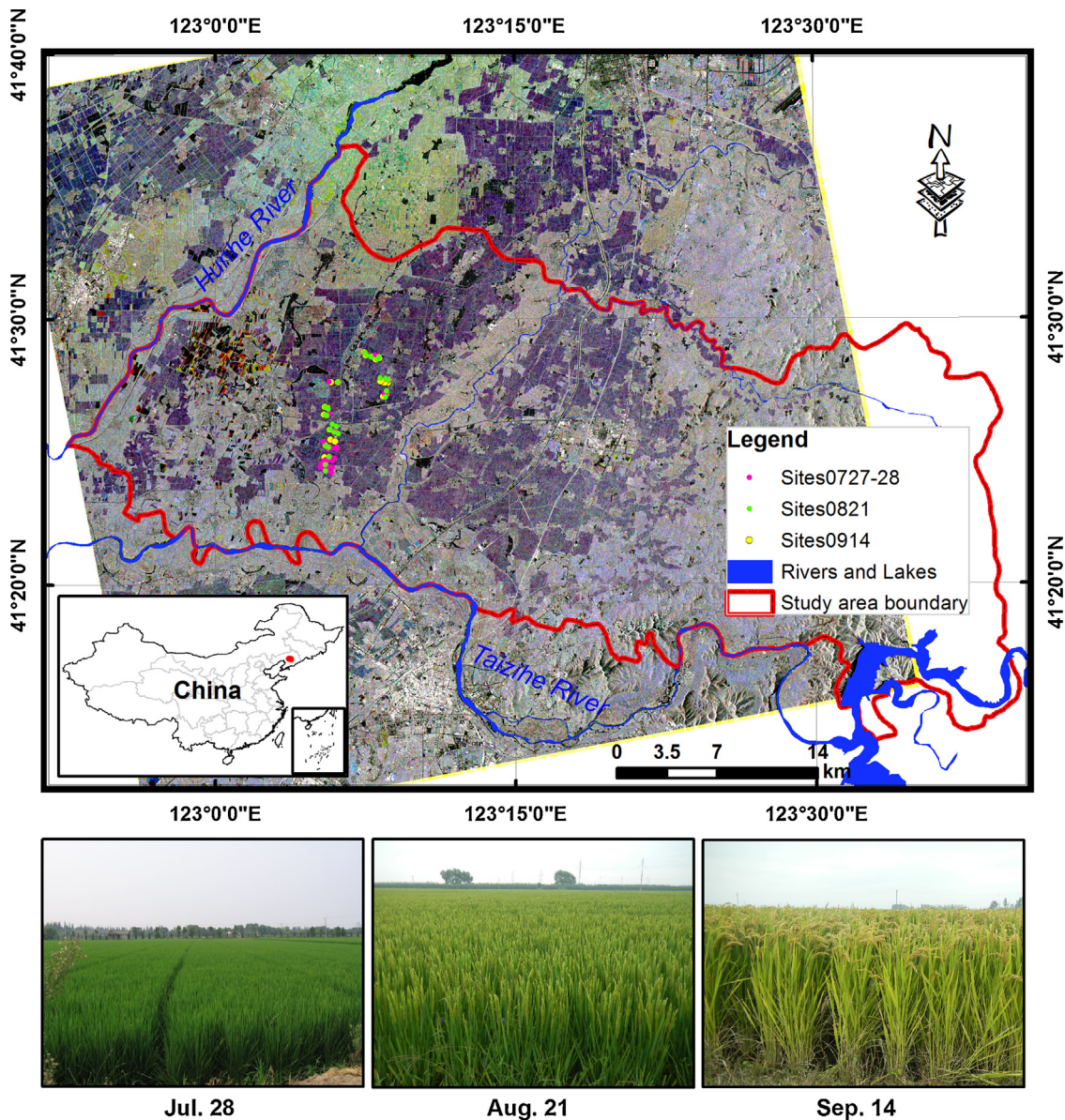


Fig. 1. Study area (Dengta City) and Radarsat-2 images acquired in three dates: Jul. 28 (R), Aug. 21 (G) and Sep. 14 (B), 2011. The sample sites visited in the corresponding dates were also marked in the figure. Photos at the bottom represent rice fields in each stage.

2.2.2. Field measurements

Field measurements synchronous to the three Radarsat-2 SAR observations were collected. A total of 85 sample sites (35 on Jul. 28, 25 on Aug. 21 and 25 on Sep. 14, 2011) were selected to measure rice biophysical parameters. Nearly half dataset measured at 44 sites (18 on Jul. 28, 13 on Aug. 21 and 13 on Sep. 14) were used for model parameterization/calibration, and the remaining half (17 on Jul. 28, 12 on Aug. 21 and 12 on Sep. 14) for validation of model simulated results. All sample sites were geo-referenced using a global positioning system (GPS) instrument. At each sample site, 10 biophysical parameters were observed: ear size (length and radius), leaf size (half-length, half-width and half-thickness) and stem size (length and radius), number of leaves per plant, and plant density and height of rice clumps (Table 1). Each parameter was an average of 5 measurements within a 1 m × 1 m unit area. Leaf insertion angle of rice plant was also measured to formulate the probability of leaf angle distribution. The rice leaf was more vertical at elongation stage than at heading and yellow ripening stage, the measured leaf insertion angles on Jul. 28 ranged from 1° to 26° (Fig. 3A), while

7° to 35° after heading (Aug. 21 and Sep. 14) (Fig. 3B and C). This indicated the necessity to separately construct PDF of rice leaves in canopy scattering model for each rice growth stage.

Sampled rice plants were cut down at each site, and the fresh weight and dry weight were weighted. The gravimetric moisture fraction (m_g) of rice plants was calculated as:

$$m_g = 1 - \frac{w_d}{w_f} \quad (1)$$

where w_d and w_f is the dry weight and fresh weight of sampled rice plants, respectively. Moisture fraction of ear layer was also calculated in the 2nd and the 3rd stages, respectively.

The gravimetric moisture fractions of rice layers were used to compute the complex dielectric constants for each layer in the Debye–Cole dual-dispersion model (Ulaby and El-Rayes, 1987), which were of great importance in simulating radar backscatter.

In the first two stages (Jul. 28 and Aug. 21), the underlying ground layer was water surface with complex dielectric constant of (80.24, −23.89i) in the C-band at ground temperature of 30 °C.

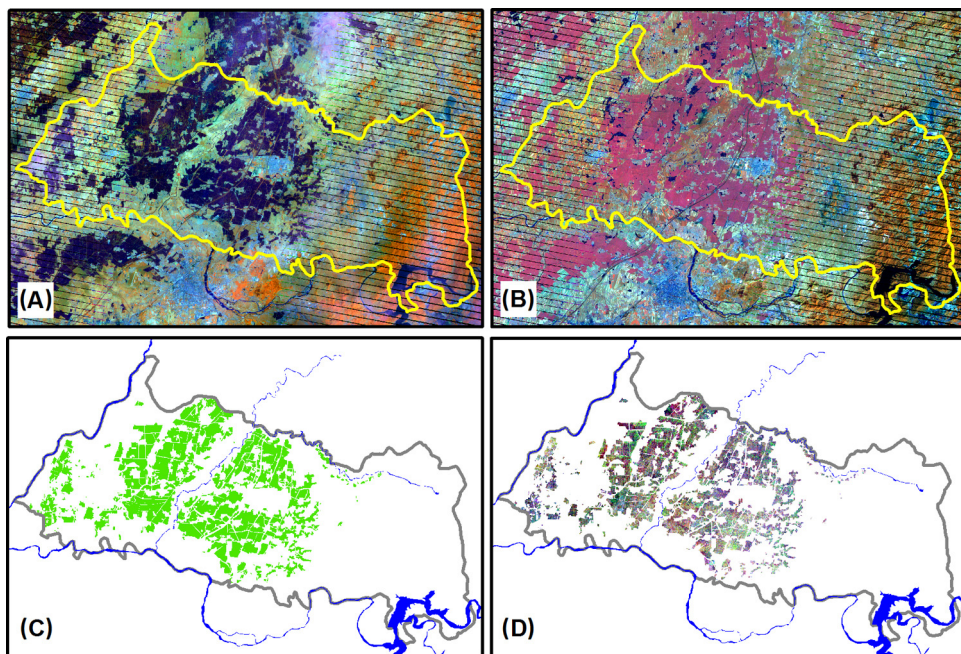


Fig. 2. The ETM+ Images (band 4, 5, 3 as R, G, B) acquired on transplanting (A) and maturation (B) stages. The rice map (C) was visually interpreted from the ETM+ images, and was used to mask rice fields from Radarsat-2 imagery (D).

Rice was becoming mature on Sep. 14 and therefore, there was no standing water covering ground surface in rice fields. Soil moisture content, however, was still high. In this study, we assumed a constant soil moisture content of $\sim 0.5 \text{ mg}$, which corresponded to a

complex dielectric constant of $(46.50, -13.08i)$ upon an empirical model (Hallikainen et al., 1985).

All these measured and calculated parameters on 85 sites during three growth stages were important inputs to parameterize and validate the canopy scattering model in this study.

2.3. Methods

2.3.1. Modeling rice backscatter

Scattering characteristics of vegetation canopy are controlled by the dielectric properties and geometric distributions of canopy components as well as the underlying ground surfaces. At the three rice growth stages, backscattering coefficients vary with canopy component size and moisture content (Inoue et al., 2002).

In our previous study, a rice canopy scattering model (RCSM) based on radiative transfer theory has been developed (Wang et al., 2009). In that model, rice canopy was simplified as the composition of three components (i.e. ear layer, leaf layer and stem layer), where the length of ear was zero prior to the heading stage (Fig. 4). Ears and stems were treated as short cylinders with finite length. For C-band radar signals, the leaf layer was the dominant contributor to the total backscattering intensity, which was simulated as a combination of long, slim ellipses with three semi-axis of length (r_a), width (r_b) and thickness (r_c), with $r_a \gg r_b \gg r_c$. Leaf volume scattering was an additive contribution from all leaves in paddy field. Detailed calculation on volume scattering of leaf, ear and stem was described in previous study (Karam et al., 1995; Wang et al., 2009). Ground surface scattering was simulated by an integral equation model (IEM) (Fung et al., 1992). Owing to the relatively calm water surface or flat soil surface during the rice growth stages, the Gaussian correlation was selected as surface correlation function for calculating ground surface scattering. In the RCSM, total backscattering intensity (σ_{total}) was a linear composition of volume scattering of each component (σ_{ear} , σ_{leaf} and σ_{stem}), its double-bounce with ground surface ($\sigma_{ear-ground}$, $\sigma_{leaf-ground}$ and $\sigma_{stem-ground}$), and surface scattering of ground (σ_{ground}) (as listed in Fig. 4):

$$\begin{aligned} \sigma_{total} = & \sigma_{ear} + \sigma_{ear-ground} + \sigma_{leaf} + \sigma_{leaf-ground} \\ & + \sigma_{stem} + \sigma_{stem-ground} + \sigma_{ground} \end{aligned} \quad (2)$$

Fig. 3. Leaf insertion angle of rice plant on Jul. 28 (A), Aug. 21 (B) and Sep. 14 (C), 2011.

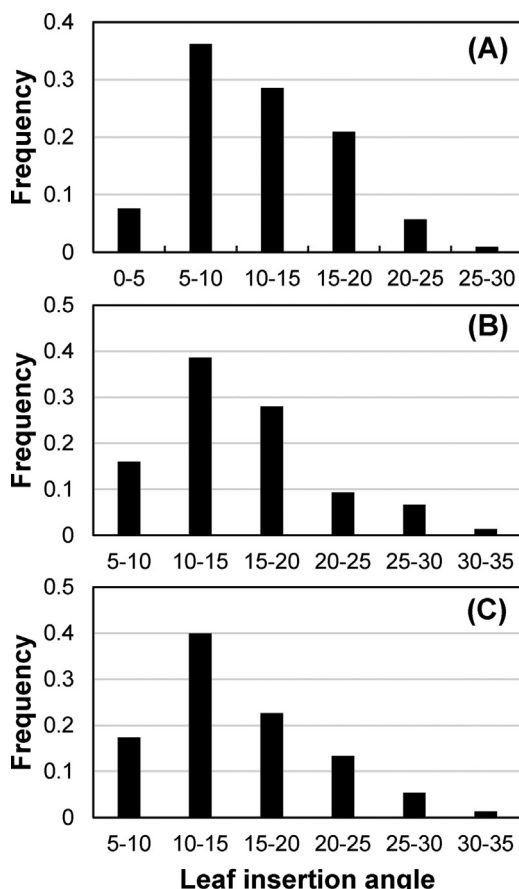


Table 1

Field-measured rice biophysical parameters for RCSM calibration.

| Physical parameters | | Jul. 28 | Aug. 21 | Sep. 14 |
|-------------------------------|------|--|------------------|------------------|
| Ear | | | | |
| Length (m) | | – | 0.15–0.18 | 0.13–0.18 |
| Radius (cm) | | – | 0.45–0.75 | 0.75–1.00 |
| Moisture gravimetric fraction | | – | 0.53–0.65 | 0.23–0.35 |
| Dielectric constant | Min. | – | (15.40, –6.74i) | (4.37, –2.51i) |
| | Max. | – | (21.70, –4.56i) | (8.12, –1.20i) |
| Leaf | | | | |
| Length (m) | | 0.16–0.23 | 0.14–0.23 | 0.13–0.19 |
| Width (cm) | | 0.80–1.00 | 0.65–1.05 | 0.80–0.95 |
| Thickness (mm) | | 0.11–0.12 | 0.13 | 0.13–0.17 |
| Density (#/m ²) | | 1152–2000 | 1035–1600 | 1008–1781 |
| Height (m) | | 0.50–0.76 | 0.75–0.98 | 0.78–0.96 |
| Moisture gravimetric fraction | | 0.70–0.83 | 0.65–0.76 | 0.57–0.69 |
| Dielectric constant | Min. | (25.04, –9.84i) | (22.91, –9.04i) | (17.66, –7.20i) |
| | Max. | (33.56, –7.35i) | (30.13, –7.06i) | (24.30, –5.43i) |
| Stem | | | | |
| Radius (cm) | | 0.35–0.45 | 0.35–0.45 | 0.35–0.45 |
| Length (m) | | 0.04–0.19 | 0.09–0.25 | 0.13–0.30 |
| Density (#/m ²) | | 272–400 | 224–400 | 233–445 |
| Moisture gravimetric fraction | | 0.70–0.83 | 0.65–0.76 | 0.57–0.69 |
| Dielectric constant | Min. | (25.04, –9.84i) | (22.91, –9.04i) | (19.06, –7.08i) |
| | Max. | (33.56, –7.35i) | (30.13, –7.06i) | (23.77, –5.82i) |
| Ground | | | | |
| Dielectric constant | | (80.24, –23.89i) | (80.24, –23.89i) | (46.50, –13.08i) |
| Roughness | | rms height: 0.015 cm; coherent length: 20 cm | | |

The RCSM was able to characterize multi-polarization rice canopy scattering at various frequencies, polarizations and incidence angles. In that previous study, the model had been applied to simulate rice scattering at the same system factors as ALOS/PALSAR (L-band, dual-polarized (HH&HV), incidence angle ranging from 36.7° to 38.5°). An identical possibility distribution function (PDF) of rice leaves was used in model for both peak tillering stage and heading stage while virtual PDF in each of growth stages is different. Simulation error of ~3 dB was thus observed for both of two stages (Wang et al., 2009). In this present study, three PDFs were constructed by leaf angles distribution measured in rice elongation, heading and yellow ripening stage, respectively. The RCSM was performed separately for the three stages, and then simulated results were validated with the C-band (5.405 GHz), dual-polarized (HH&HV) Radarsat-2 observation with incidence angle of 33.5°.

From the in situ measurements, the above-water canopy height of rice plants ranged within [0.6 m, 0.9 m], [0.95 m, 1.25 m], [1.0 m, 1.2 m] on the three stages. The plant density ranged within [250, 400] on Jul. 28, and same range [250, 350] on the other two observation dates. Given these boundary conditions, the optimal physical

parameters (rice height and density) would be estimated using an effective optimization tool.

2.3.2. Genetic algorithm (GA) for retrieving biophysical parameters

The genetic algorithm (GA) is a variable screening procedure, and it analyzes the process of natural selection based on the principle of evolutionary genetics (Holland, 1975). A most important advantage is the GA provides a systematic scanning of the whole population, so a global optimum solution could be identified avoiding being stuck on a local maxima or minima (De Castro and Cavalca, 2003). Another advantage is that GA avoids the initial guess selection problem. Although with the limitation in expensive computational cost, the GA is generally more efficient than gradient search methods if the search space has many local optima. As a robust method, GA was widely used spectral features selection of remote sensing imagery (Van Coillie et al., 2007), image fusion, fragmentation and classification (Tso and Mather, 1999; Garzelli and Nencini, 2006), retrieval of vegetation canopy biophysical parameters and land surface roughness and soil moisture (Fang et al., 2003; Jin and Wang, 1999), and detection of oil spilled on the sea surface

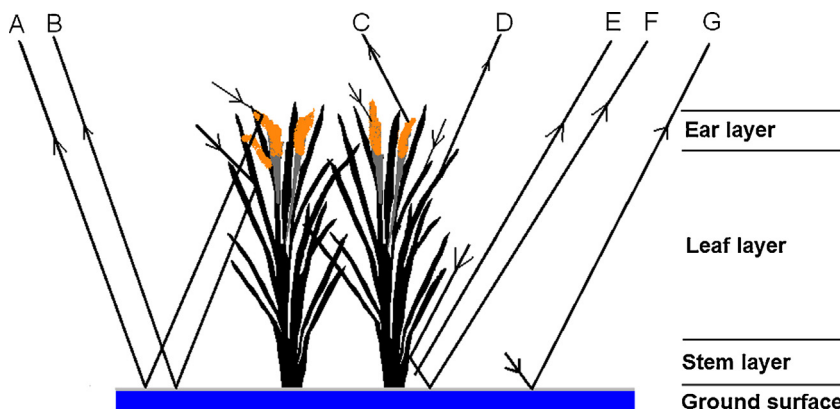


Fig. 4. Geometry of rice canopy and scattering components: (A) ear-ground interaction ($\sigma_{\text{ear-ground}}$); (B) leaf-ground interaction ($\sigma_{\text{leaf-ground}}$); (C) ear volume scattering (σ_{ear}); (D) leaf volume scattering (σ_{leaf}); (E) stem volume scattering (σ_{stem}); (F) stem-ground interaction ($\sigma_{\text{stem-ground}}$); and (G) ground surface scattering (σ_{ground}).

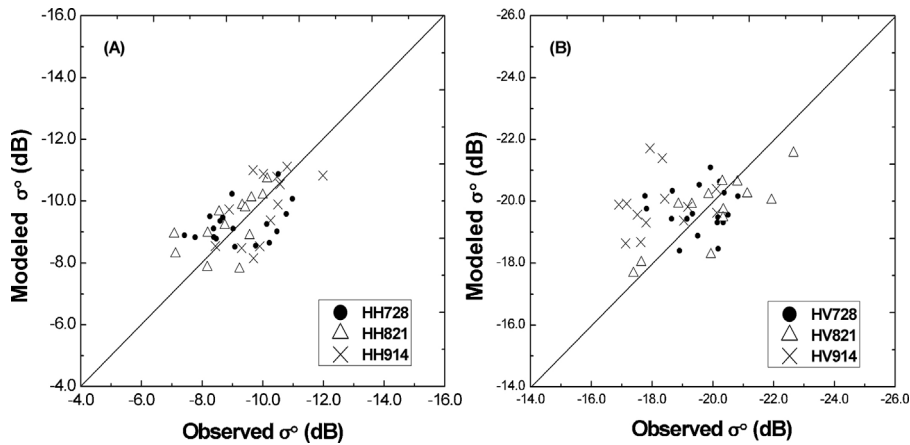


Fig. 5. Scatterplots of the RCSM modeled vs. Radarsat-2 observed backscattering coefficients (σ°) in HH (A) and HV (B) polarizations.

(Jubai et al., 2006). These studies successfully demonstrated the potential of GA to a variety of optimization problems in remote sensing applications.

In this study, the genetic algorithms for optimization toolbox (GAOT) (Houck et al., 1996) was used to perform the identification of optima within the given search spaces of rice physical parameters. By integrating the RCSM and GAOT at the MATLAB environment, canopy height and density of paddy rice in the three stages were extracted via model inversion from the Radarsat-2 SAR images.

2.3.3. Model validation and accuracy assessment

After an elaborate parameterization process, model performance was evaluated by comparing the simulated backscatter (modeled σ°) at validated sites with that from the Radarsat-2 SAR images (observed σ°).

Statistical measures of the mean absolute error (MAE) and root mean square error (RMSE) were adapted to assess the “goodness of fit” of model simulations. The two measures were calculated as below:

$$\text{MAE} = \frac{1}{n} \sum_{i=1}^n |X_{\text{modeled}}^i - X_{\text{observed}}^i| \quad (3)$$

$$\text{RMSE} = \sqrt{\frac{\sum_{i=1}^n (X_{\text{modeled}}^i - X_{\text{observed}}^i)^2}{n}} \quad (4)$$

where, n is the total number of ground samples, X_{observed}^i is the observed value and X_{modeled}^i is the modeled/retrieved value. Both RCSM model simulation and biophysical retrieval were evaluated with these two statistical measures.

3. Results

3.1. Modeled rice backscatter

To be consistent with the RASARSAT-2 system configuration, only dual-polarization (HH&HV) scattering in the C-band (frequency of 5.405 GHz) at incidence angle of 34° were simulated in the RCSM. In the three growth stages at the sampled sites, the modeled σ° of rice canopy ranges from −7.0 dB to −12.0 dB for HH and from −17.0 dB to −22.0 dB for HV polarization (Fig. 5). For each of validation site, the number value (σ°) at corresponding pixel of resampled Radarsat-2 images (resolution of 30 m × 30 m) was abstracted. The observed σ° at validation site was then compared against model simulations at the field scale. The RCSM simulations reasonably matched the Radarsat-2 observed backscattering

coefficients for both HH and HV polarization. The modeled HH backscattering coefficients were closer to SAR observations than HV. Samples in the HH scatterplot coefficients were very close to the 1:1 line (Fig. 5A), while those in the HV scatterplot showed a greater dispersion (Fig. 5B). On Sep. 14, the simulated HV backscatter values were approximately 2 dB lower than the Radarsat-2 observations. The biggest simulation errors were of 1.77 dB of MAE and 2.03 dB of RMSE. Higher simulation accuracy (no more than 1.0 dB for both HH and HV) was observed in HH backscatter in rice heading stage (Aug. 21). Statistical analysis demonstrated that both MAE and RMSE for HH backscatter were less than those of HV (Table 2). The MAE and RMSE of modeled HH values were less than 1.0 dB when all three stages were considered. Therefore in this study, the HH data were selected as the input of RCSM for retrieving height and density of rice canopy.

Rice backscatter varied with biophysical parameters in paddy fields (Table 3). Sensitivity analysis was conducted to examine the contribution of each parameter in the simulated backscattering coefficients in the RCSM. When certain biophysical parameter was examined, other parameters were assumed constant as listed in Table 3.

Ears were important structural components in rice heading stage. The modeled backscatter increased with increasing moisture content of rice ear while decreased with increasing ear size in the near-maturation stage (Sep. 14). In this stage, rice ear became an attenuator to SAR signals. Its dielectric constants were small due to its low moisture contents. However in the early-heading stage (Aug. 21), the modeled backscatter was not very sensitive. The ear layer with high dielectric property was an important contributor to total volume scattering of rice canopy (Fig. 6A–C).

Leaf layer is the dominant scatter in all of the three growth stages. Its backscatter increased with increasing leaf dimension such as leaf length (Fig. 6D), width (Fig. 6E) and thickness (Fig. 6F) and increasing moisture content (Fig. 6H). In the elongation and heading stages, total backscatter firstly decreased with increasing leaf layer height and then reached saturation. In the yellow ripening stage, leaf layer height had little impacts on total backscatter,

Table 2

Accuracy evaluation (MAE and RMSE) for modeled backscattering coefficients (unit: dB) in the three rice growing stages.

| Date | Site numbers | MAE | | RMSE | |
|---------|--------------|------|------|------|------|
| | | HH | HV | HH | HV |
| Jul. 28 | 18 | 0.90 | 0.94 | 1.00 | 1.12 |
| Aug. 21 | 13 | 0.77 | 0.78 | 0.90 | 0.94 |
| Sep. 14 | 13 | 0.81 | 1.77 | 0.91 | 2.03 |
| Total | 44 | 0.89 | 1.99 | 0.94 | 1.41 |

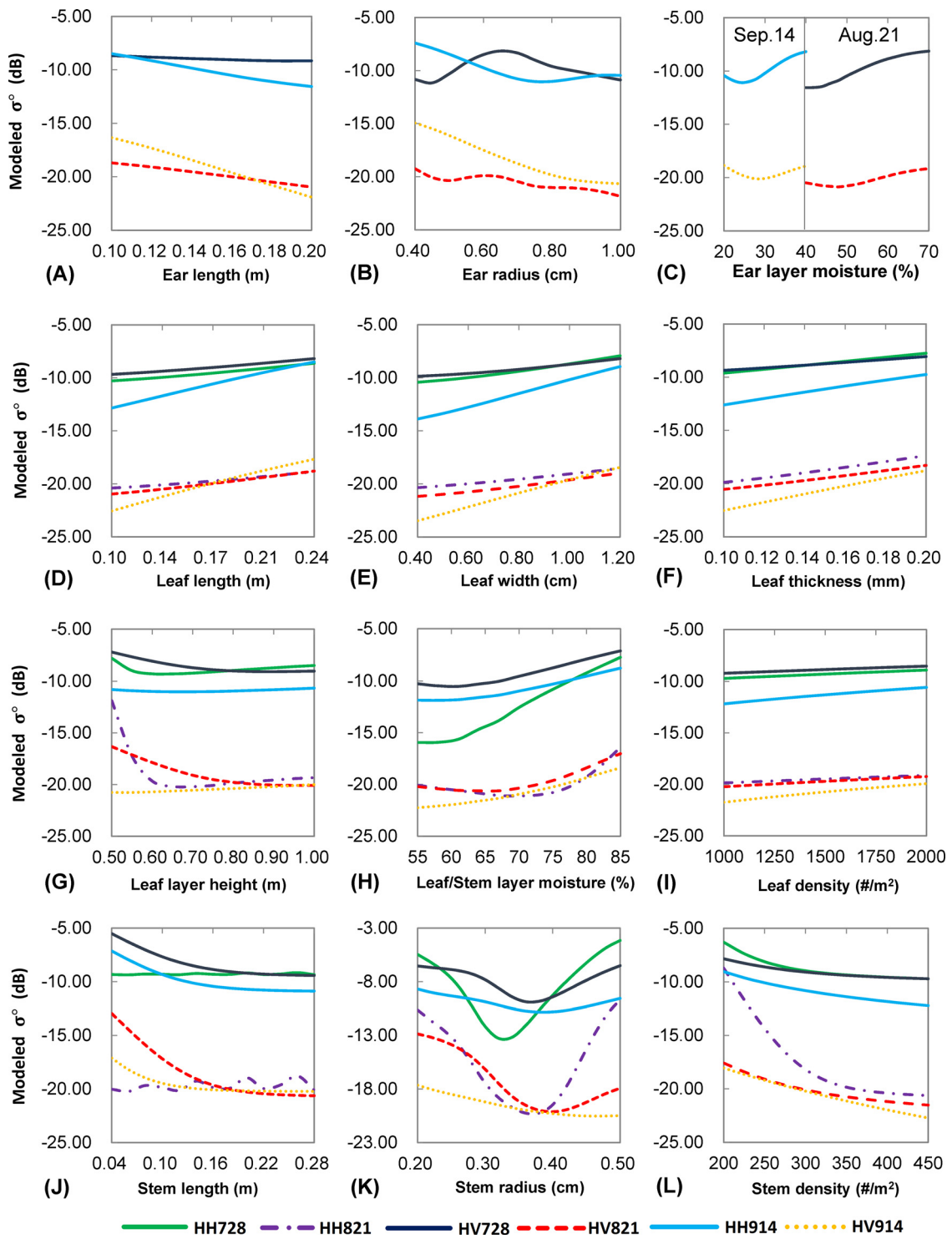


Fig. 6. RCSM simulation of the contribution of rice physical parameters on total backscattering coefficients.

which may be mainly contributed to the lower moisture content at this stage (Fig. 6G). Leaf density of rice clumps had a slightly positive effect on total backscatter after the peak tillering stage (Fig. 6I).

In elongation stage before ears emerged, total backscatter was not sensitive to stem length. When ears started to emerge (small ears), total backscatter gradually decreased and tended to saturate with the developing stem (Fig. 6J). There was large variability in total backscatter responding to stem radius and a decreasing trend was observed for HV polarization at yellow ripening stage on Sep. 14 (Fig. 6G). Evidently decreasing trends in total backscatter were

observed with the increasing stem density due to strong extinction (Fig. 6L).

Total HH-polarization backscatter and the contribution of different components in the RCSM were shown in Fig. 7 with the change of leaf layer height and plant density. Plant height was positively related to leaf layer height. All other parameters were assumed constant, as listed in Table 4. With the RCSM, ear volume scattering and leaf volume scattering were larger than -20 dB. This indicated that the two major scattering components that contributed to the total backscatter in HH polarization. Although stem volume

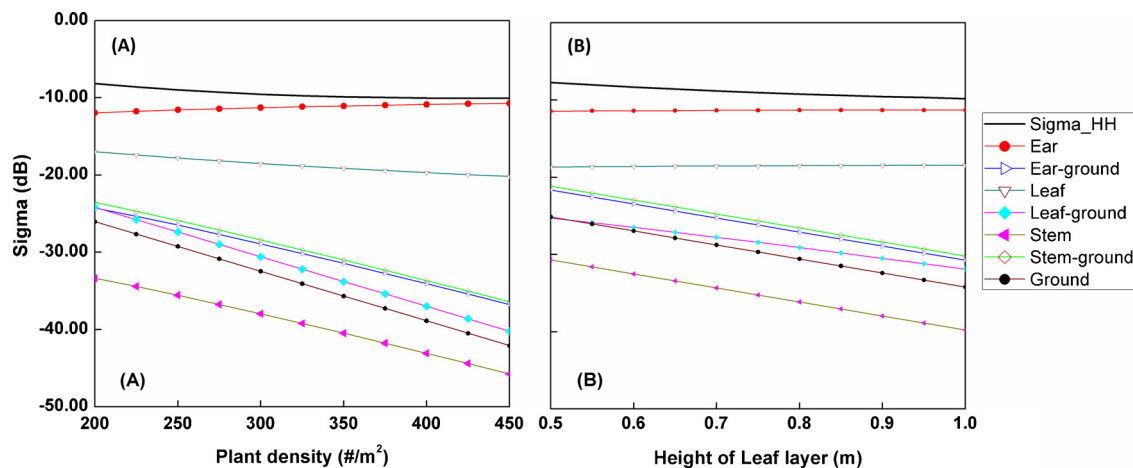


Fig. 7. Contribution of scattering components to the total rice backscatter in HH that varied with (A) leaf layer height and (B) plant density.

Table 3
Rice biophysical parameters for sensitivity analysis of RCSM.

| Physical parameters | Range tested |
|-------------------------------|----------------------------------|
| Ear | |
| Length (m) | 0.10–0.20 |
| Radius (cm) | 0.40–1.00 |
| Moisture gravimetric fraction | 0.20–0.70 |
| Complex dielectric constant | (3.70, −0.94i)–(24.79, −7.41i) |
| Leaf | |
| Length (m) | 0.10–0.24 |
| Width (cm) | 0.40–1.20 |
| Thickness (mm) | 0.10–0.20 |
| Density (#/m ²) | 1000–2000 |
| Layer height (m) | 0.50–1.00 |
| Moisture gravimetric fraction | 0.55–0.85 |
| Complex dielectric constant | (16.49, −5.09i)–(34.95, −10.14i) |
| Stem | |
| Length (m) | 0.20–0.50 |
| Radius (cm) | 0.04–0.28 |
| Density (#/m ²) | 200–450 |
| Moisture gravimetric fraction | 0.55–0.85 |
| Complex dielectric constant | (16.49, −5.09i)–(34.95, −10.14i) |

scattering was less than -30 dB, it was slightly larger than ear and leaf double bounce. All three double bounce scattering reduced with increasing plant density and leaf height because of stronger attenuation when radar signals interacted with ears and leaves. Direct ground scattering from smooth water surface was negligible, these scattering components were not shown in Fig. 7. Scattering

from ground surface without covered by standing water was simulated in the yellow ripening stage (Sep. 14). The soil gravimetric moisture fraction was ~ 0.5 of (m_g) that correspond to complex dielectric constant of (46.50, $-13.08i$). The flat soil surface in rice fields presented similar changing behavior to the double bounce scattering of rice components. Plant density made more effect to ground scattering than leaf height (Fig. 7A).

3.2. Retrieval of rice canopy height and density

As shown in Fig. 5, the RCSM simulation of HH backscatter matched the Radarsat-2 observations better than that of HV backscatter, especially in rice maturation stage. Therefore, the HH data were used to estimate rice canopy height and density in this study. Other rice parameters were assumed constant in each stage. Considering biophysical variations along with rice development, these parameters were given different set of values in each of the three stages examined in this study (Table 4).

At the environment of MATLAB, model inversion of rice height and density was performed by integrating the parameterized RCSM and GAOT. Only backscatter in paddy fields was considered in model inversion. For each parameter, three outputs were produced from three HH backscattering coefficient images (Fig. 8). For the entire study area, the estimated rice height varied in the range of 20–30 cm while plant density was from 100 to 150 #/m². Larger variation appeared in the rice elongation stage Jul. 28, which might come from different agricultural practices (e.g. transplanting date and fertilizer application) or rice cultivars (Fig. 8A1 and B1). Temporally, rice in the rice elongation stage was shorter than other two stages (Aug. 21 and Sep. 14) (Fig. 8A2 and A3). Rice density kept relatively stable because the tillering was terminated after the rice elongation stage. During growing season, plant density could be decreased because of nutrient competition among individual plants (Fig. 8B2 and B3).

The retrieved results in the three stages were validated with the field measurements at the sample sites in each corresponding stage. When all three stages were considered, rice height could be retrieved from Radarsat-2 HH image with MAE of 4.5 cm and RMSE of 5.4 cm, and rice density has MAE of 21 #/m² and RMSE of 26 #/m² (Fig. 9). The retrieved height parameters at heading stage (Aug. 21) and density parameters at yellow ripening stage (Sep. 14) showed the highest agreement with the in situ measurements (Fig. 9A2 and C2), with a MAE of 2.6 cm and 4 #/m² and RMSE of 13.3 cm and 17 #/m², respectively. This showed that the retrieval of rice biophysical parameters after the heading stage could be performed

Table 4
Specified inputs to RCSM for rice height and density inversion.

| Physical parameters | Jul. 28 | Aug. 21 | Sep. 14 |
|-----------------------------|---|---------------------|---------------------|
| Ear | | | |
| Length (m) | – | 0.16 | 0.17 |
| Radius (cm) | – | 0.56 | 0.85 |
| Dielectric constant | – | (18.20, $-5.53i$) | (6.02, $-1.80i$) |
| Leaf | | | |
| Length (m) | 0.19 | 0.17 | 0.16 |
| Width (cm) | 0.84 | 0.86 | 0.9 |
| Thickness (mm) | 0.12 | 0.13 | 0.16 |
| Density (#/m ²) | 1518 | 1174 | 1808 |
| Dielectric constant | (31.34, $-9.09i$) | (26.86, $-7.87i$) | (27.77, $-8.11i$) |
| Stem | | | |
| Length (m) | 0.11 | 0.18 | 0.24 |
| Radius (cm) | 0.40 | 0.41 | 0.39 |
| Dielectric constant | (31.34, $-9.09i$) | (26.86, $-7.87i$) | (21.66, $-6.47i$) |
| Ground | | | |
| Dielectric constant | (80.24, $-23.89i$) | (80.24, $-23.89i$) | (46.50, $-13.08i$) |
| Roughness | rms height: 0.15 mm; coherent length: 20 cm | | |

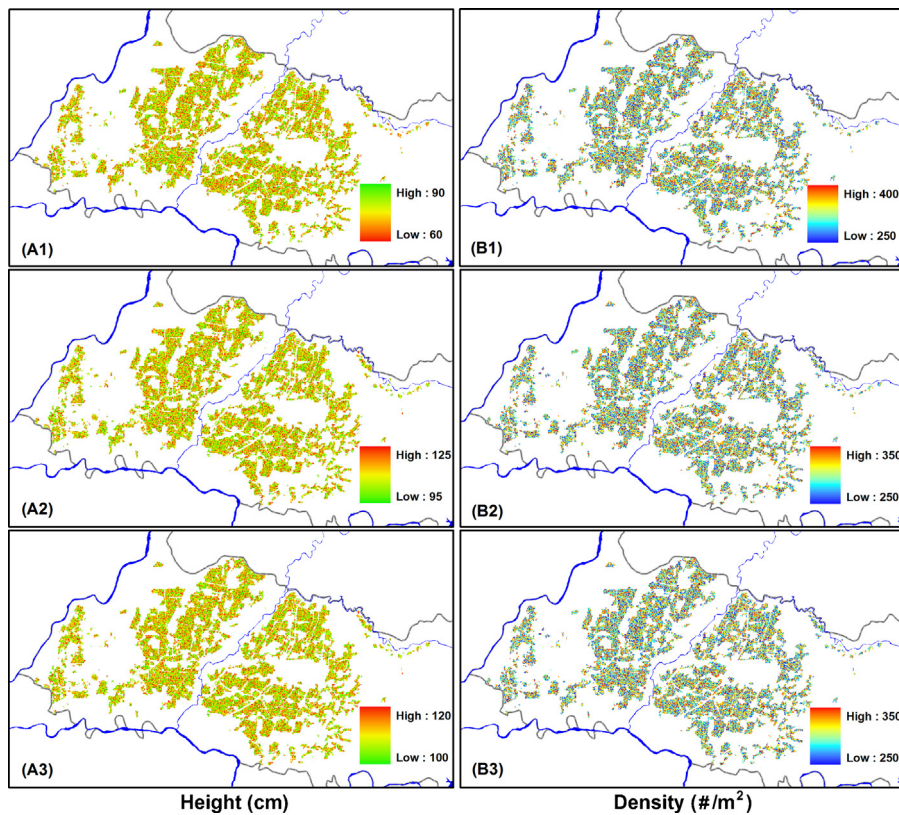


Fig. 8. Spatial distributions of rice height and density retrieved from Rardarsat-2 HH data at three rice growth stages.

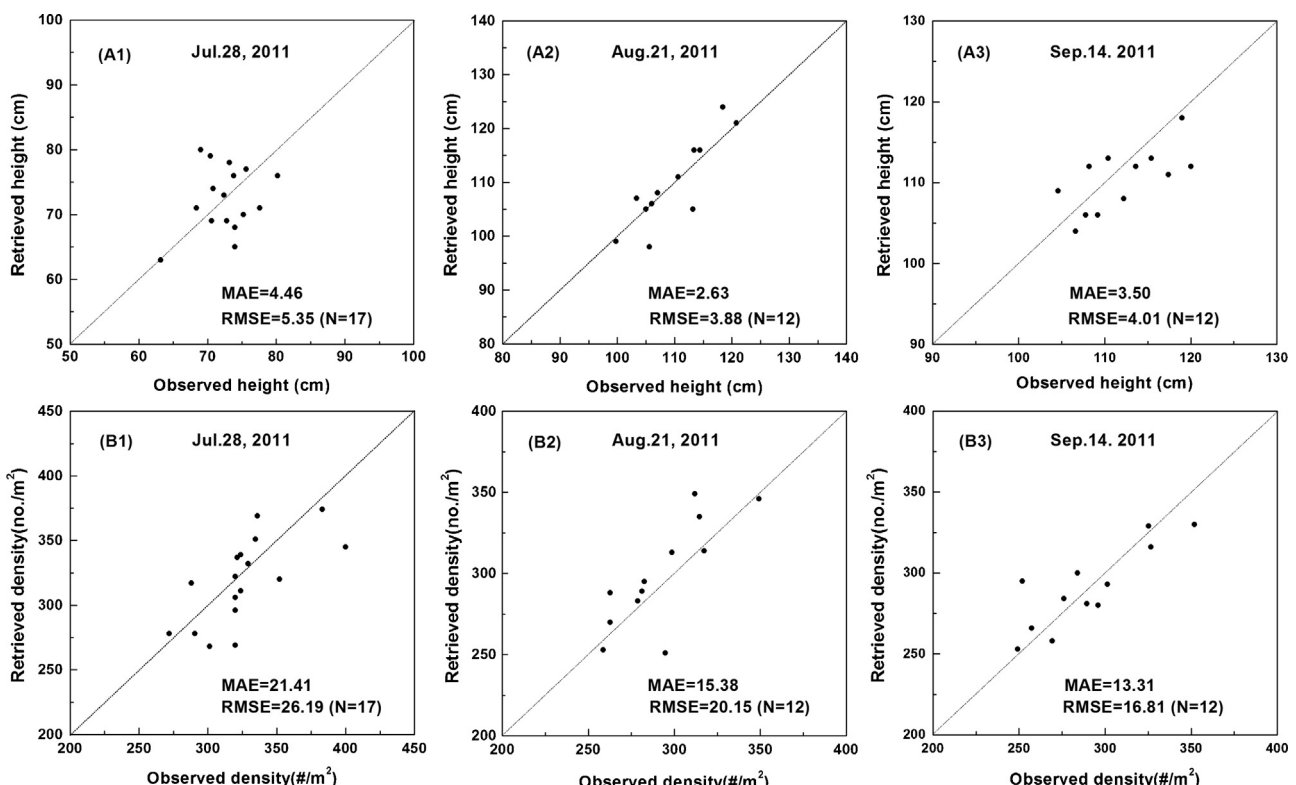


Fig. 9. Retrieved vs. observed rice height (A1, A2 and A3) and density (B1, B2 and B3) at three rice growth stages.

more accurately, indicating the high potential of Radarsat-2 SAR data to rice monitoring in these stages.

4. Discussions

Effective simulation of backscattering coefficients of rice canopy is crucial to the retrieval of rice biophysical parameters. In our previous study reported in Wang et al. (2009), rice parameters observed in two stages (peak tillering and heading) were synthetically analyzed without taking into account the parameters variations along with rice development. Large inconsistency in simulated and satellite observed backscattering coefficients could be explained by this parameterization method. Therefore in this study, we substantially analyzed vegetative elements size and probability distribution feature of rice canopy in the three stages (elongation, heading and yellow ripening). The scattering behaviors in each of the three stages were separately simulated by specifying unique set of values in RCSM based on elaborative field measurements. The performance of RCSM was evidently improved from previous works (with MAE and RMSE <1 dB for C-band HH data). In this present study, only dual-polarization C-band data (HH and HV) were acquired for validating the RCSM-simulated results, we did not test RCSM's capability in simulating scattering characteristics of rice canopy at other polarization modes (i.e. VH, VV). Fortunately, full-polarization Radarsat-2 data (HH, HV, VH and VV) is available for users, the future efforts will be made to further investigate the performance of RCSM for rice microwave remote sensing.

In the rice yellow ripening stage (Sep. 14), the RCSM-modeled σ^0 is ~2 dB larger than imagery-observed σ^0 for HV data (Fig. 5B). This disagreement could be attributed to the parameter setting. We set identical soil moisture for all the rice fields while there are large variations for actual field conditions. This inevitably introduces uncertainty into total backscatter of rice canopy as co-polarization (HV) is more sensitive than cross-polarization (HH) soil moisture variations (McNairn and Brisco, 2004). This suggests that for rice mature stage, the scattering contribution from the underlying surface to total backscattering should not be neglected, and detailed field observation is necessary for obtaining better simulation accuracy.

As far as the retrieval of rice biophysical parameters is concerned, efficient and effective retrieval is depend on not only the model performance, but also the robustness of optimization algorithm. In this study, although the GAOT is effective for parameters searching within given ranges, the computing cost is so expensive for high resolution radar image over large study area. Further work will focus on the selection of efficient retrieval tools such like artificial neural network (ANN). Thus it might extend the practical application of SAR remote sensing to rice growth monitoring and biomass estimation at regional scale, which is very helpful for the decision making of agriculture management.

5. Conclusions

In this study, two rice physical parameters, canopy height and density, were estimated from the C-band Radarsat-2 SAR data with the integration of a rice canopy scattering model (RCSM) and optimization toolbox GAOT. Major findings include:

- (1) The scattering model based on the radiative transfer equation has great potential to interpret complex interactions of radar with rice canopy components. For dual-polarization (HH and HV) C-band SAR signal, the RCSM was able to effectively simulate the scattering characteristics at three growth stages of rice with MAE and RMSE <2 dB.

- (2) In this study, rice canopy height and density were retrieved with approximate RMSE of 5.4 cm and 26#/m². The retrieval was most effective in the heading stage, the RMSE of rice canopy height and density is 3.8 cm and 19#/m², respectively.
- (3) The C-band, HH-polarized Radarsat-2 SAR imagery would be more promising data source for rice biophysical quantification and growth monitoring at regional scale.

Acknowledgements

This research was primarily supported by National Natural Science Foundation of China (Grant No. 41001202), and partly funded by the Foundation for Innovative Research of East China Normal University.

References

- Bouvet, A., Le Toan, T., 2011. Use of ENVISAT/ASAR wide-swath data for timely rice fields mapping in the Mekong River Delta. *Remote Sensing of Environment* 115 (4), 1090–1101.
- Chakraborty, M., Manjunath, K.R., Panigrahy, S., Kundu, N., Parihar, J.S., 2005. Rice crop parameter retrieval using multi-temporal, multi-incidence angle Radarsat SAR data. *ISPRS Journal of Photogrammetry and Remote Sensing* 59(5), 310–322.
- Chen, J., Lin, H., Liu, A., Shao, Y., Yang, L., 2006. A semiempirical backscattering model for estimation of leaf area index (LAI) of rice in southern China. *International Journal of Remote Sensing* 27 (24), 5417–5425.
- De Castro, H.F., Cavalcá, K.L., 2003. Availability optimization with genetic algorithm. *International Journal of Reliability Management* 20 (7), 847–863.
- Fang, H., 1998. Rice crop area estimation of an administrative division in China using remote sensing data. *International Journal of Remote Sensing* 19 (17), 3411–3419.
- Fang, H., Liang, S., Kuusk, A., 2003. Retrieving leaf area index using a genetic algorithm with a canopy radiative transfer model. *Remote Sensing of Environment* 85 (3), 257–270.
- Frolking, S., Qiu, J., Boles, S., Xiao, X., Liu, J., Zhuang, Y., Li, C.S., Qin, X., 2002. Combining remote sensing and ground census data to develop new maps of the distribution of rice agriculture in China. *Global Biogeochemical Cycles* 16 (4), 1091.
- Fung, A.K., Lee, Z., Chen, K.S., 1992. Backscattering from a randomly rough dielectric surface. *IEEE Transactions on Geoscience and Remote Sensing* 30 (6), 799–808.
- Garzelli, A., Nencini, F., 2006. PAN-sharpening of very high resolution multispectral images using genetic algorithms. *International Journal of Remote Sensing* 27 (15), 3273–3292.
- Hallikainen, M.T., Ulaby, F.T., Dobson, M.C., El-Rayes, M.A., Wu, L.K., 1985. Microwave dielectric behavior of wet soil – Part I: empirical models and experimental observations. *IEEE Transactions on Geoscience and Remote Sensing* GE-23 (1), 25–34.
- Holland, J.H., 1975. *Adaptation in Natural and Artificial Systems*. The University of Michigan Press, Ann Arbor.
- Houck, C.R., Joines, J.A., Kay, M.G., 1996. A Genetic Algorithm for Function Optimization: A Matlab Implementation. <http://citeseerx.ist.psu.edu/viewdoc/download?doi=10.1.1.22.4413&rep=rep1&type=pdf> (accessed 10.09.13).
- Inoue, Y., Kurosu, T., Maeno, H., Uratsuka, S., Kozu, T., Dabrowska-Zielinska, K., Qi, J., 2002. Season-long daily measurements of multifrequency (Ka, Ku, X, C, and L) and full-polarization backscatter signatures over paddy rice field and their relationship with biological variables. *Remote Sensing of Environment* 81 (2–3), 194–204.
- Jin, Y., Wang, Y., 1999. A genetic algorithm to simultaneously retrieve land surface roughness and soil wetness. *International Journal of Remote Sensing* 22 (15), 3093–3099.
- Jubai, A., Jing, B., Yang, J., 2006. Combining fuzzy theory and a genetic algorithm for satellite image edge detection. *International Journal of Remote Sensing* 27 (14), 3013–3024.
- Karam, A.M., Amar, F., Fung, K.A., Mougin, E., Lopes, A., Le Vine, M.D., Beaudoin, A., 1995. A microwave polarimetric scattering model for forest canopies based on vector radiative transfer theory. *Remote Sensing of Environment* 53 (1), 16–30.
- Koppe, W., Gnyp, M.L., Hütt, C., Yao, Y., Miao, Y., Chen, X., Bareth, G., 2013. Rice monitoring with multi-temporal and dual-polarimetric TerraSAR-X data. *International Journal of Applied Earth Observation and Geoinformation* 21, 568–576.
- Le Toan, T., Laur, H., Mougin, E., Lopes, A., 1989. Multitemporal and dual-polarization observations of agricultural vegetation covers by X-band SAR images. *IEEE Transactions on Geoscience and Remote Sensing* 27 (6), 709–717.
- Le Toan, T., Ribbes, F., Wang, L.F., Nicolas, F., Ding, K.H., Kong, J.A., Fujita, M., Kurosu, T., 1997. Rice crop mapping and monitoring using ERS-1 data based on experiment and modeling results. *IEEE Transactions on Geoscience and Remote Sensing* 35 (1), 41–56.
- Li, Y., Liao, Q., Li, X., Liao, S., Chi, G., Peng, S., 2003. Towards an operational system for regional-scale rice yield estimation using a time-series of Radarsat ScanSAR images. *International Journal of Remote Sensing* 24 (21), 4207–4220.
- Lin, C.S., Ho, P.S., 2003. China's land resources and land-use change: insights from the 1996 land survey. *Land Use Policy* 20 (2), 87–107.

- Lopes, A., Nezry, E., Touzi, R., Laur, H., 1990. Maximum a posteriori filtering and first order texture models in SAR images. In: Proceedings of IEEE Geoscience and Remote Sensing Symposium, Vol. 3, Maryland, USA, 20–24 May, pp. 2409–2412.
- McNairn, H., Brisco, B., 2004. The application of C-band polarimetric SAR for agriculture: a review. *Canadian Journal of Remote Sensing* 30 (3), 525–542.
- National Bureau Statistics of China, 1990. *China Statistical Yearbook-1990*. China Statistics Press, Beijing.
- National Bureau Statistics of China, 2000. *China Statistical Yearbook-2000*. China Statistics Press, Beijing.
- National Bureau Statistics of China, 2013. *China Statistical Yearbook-2013*. China Statistics Press, Beijing.
- Nuarsa, I.W., Nishio, F., Hongo, C., Mahardika, I.G., 2012. Using variance analysis of multitemporal MODIS images for rice field mapping in Bali Province, Indonesia. *International Journal of Remote Sensing* 33 (17), 5402–5417.
- Okamoto, K., Kawashima, H., 1999. Estimation of rice-planted area in the tropical zone using a combination of optical and microwave satellite sensor data. *International Journal of Remote Sensing* 20 (3), 1045–1048.
- Oza, S.R., Panigrahy, S., Parihar, J.S., 2008. Concurrent use of active and passive microwave remote sensing data for monitoring of rice crop. *International Journal of Applied Earth Observation and Geoinformation* 10 (3), 296–304.
- Panigrahy, S., Manjunath, K.R., Chakraborty, M., Kundu, N., Parihar, J.S., 1999. Evaluation of RADARSAT standard beam data for identification of potato and rice crops in India. *ISPRS Journal of Photogrammetry and Remote Sensing* 54 (4), 254–262.
- Ribbes, F., Le Toan, T., 1999. Rice field mapping and monitoring with RADARSAT data. *International Journal of Remote Sensing* 20 (4), 745–765.
- Shao, Y., Fan, X., Liu, H., Xiao, J., Ross, S., Brisco, B., Brown, R., Staples, G., 2001. Rice monitoring and production estimation using multi-temporal Radarsat. *Remote Sensing of Environment* 76 (3), 310–325.
- Shao, Y., Liao, J., Wang, C., 2002. Analysis of temporal radar backscatter of rice: a comparison of SAR observations with modeling results. *Canada Journal of Remote Sensing* 28 (2), 128–138.
- Su, S., Jiang, Z., Zhang, Q., Zhang, Y., 2011. Transformation of agricultural landscapes under rapid urbanization: a treat to sustainability in Hang-Jia-Hu region, China. *Applied Geography* 31 (2), 439–449.
- Tsang, L., Ding, K.H., Zhang, G., Hsu, C.C., Kong, J.A., 1995. Backscattering enhancement and clustering effects of randomly distributed dielectric cylinders overlying a dielectric half space based on Monte-Carlo simulations. *IEEE Transactions on Antennas and Propagation* 43 (5), 488–499.
- Tso, B.C.K., Mather, P.M., 1999. Classification of multisource remote sensing imagery using a genetic algorithm and Markov random fields. *IEEE Transactions on Geoscience and Remote Sensing* 37 (3), 1255–1260.
- Ulaby, F.T., El-Rayes, M.A., 1987. Microwave dielectric spectrum of vegetation. Part II: dual-dispersion model. *IEEE Transactions on Geoscience and Remote Sensing* GE-25 (5), 550–557.
- Van Coillie, F.M.B., Verbeke, L.P.C., De Wulf, R.R., 2007. Feature selection by genetic algorithms in object-based classification of IKONOS imagery for forest mapping in Flanders, Belgium. *Remote Sensing of Environment* 110 (4), 476–487.
- Wang, L.F., Kong, J.A., Ding, K.H., Le Toan, T., Ribbes, F., Flouri, N., 2005. Electromagnetic scattering model for rice canopy based on Monte Carlo simulation. *Progress in Electromagnetics Research* 52, 153–171.
- Wang, C., Wu, J., Zhang, Y., Pan, G., Qi, J., Salas, A.W., 2009. Characterizing L-band scattering of paddy rice in Southeast China with radiative transfer model and multitemporal ALOS/PALSAR imagery. *IEEE Transactions on Geoscience and Remote Sensing* 47 (4), 988–998.
- Welch, R., Ehlers, W., 1987. Merging multiresolution SPOT HRV and Landsat TM data. *Photogrammetric Engineering & Remote Sensing* 53 (3), 301–303.
- Wu, J.X., Cheng, X., Xiao, H.S., Wang, H.Q., Yang, L.Z., Ellis, E.C., 2009. Agricultural landscape change in China's Yangtze Delta, 1942 and 2002: a case study. *Agriculture, Ecosystems and Environment* 129 (4), 523–533.
- Xiao, X., Boles, S., Liu, J., Zhuang, D., Froliking, S., Li, C., Salas, W., Moore III, B., 2005. Mapping paddy rice agriculture in southern China using multi-temporal MODIS images. *Remote Sensing of Environment* 95 (4), 480–492.
- Yonezawa, C., Negishi, M., Azuma, K., Watanabe, M., Ishitsuka, N., Ogawa, S., Saito, G., 2012. Growth monitoring and classification of rice fields using multitemporal RADARSAT-2 full-polarimetric data. *International Journal of Remote Sensing* 33 (18), 5696–5711.
- Zhang, Y., Wang, C., Wu, J., Qi, J., Salas, A.W., 2009. Mapping paddy rice with multi-temporal ALOS PALSAR imagery in southeast China. *International Journal of Remote Sensing* 30 (23), 6301–6315.
- Zhang, Y., Wang, C., Zhang, Q., 2011. Identifying paddy fields with dual-polarization PALSAR data. *Canadian Journal of Remote Sensing* 37 (1), 103–111.
- Zhang, Y., Su, S., Zhang, F., Shi, R., Gao, W., 2012. Characterizing spatiotemporal dynamics of methane emissions from rice paddies in northeast China from 1990 to 2010. *PLOS ONE* 7 (1), e29156.